Review of Scientific Instruments | ARTICLE | pubs.aip.org/aip/rsi

Redifining RADEN's high-resolution neutron imaging capabilities

Cite as: Rev. Sci. Instrum. 95, 113702 (2024); doi: 10.1063/5.0235243
Submitted: 26 August 2024 • Accepted: 14 October 2024 •
Published Online: 8 November 2024

View Online Export Citation CrossMark

Oriol Sans-Planell,[1,a)] Takenao Shinohara,[2] Francesco Grazzi,[3,4] Francesco Cantini,[3,4] Yuhua Su,[2] Yoshihiro Matsumoto,[2] Joseph D. Parker,[2] and Ingo Manke[1]

AFFILIATIONS

[1] Helmholtz-Zentrum Berlin für Materialen und Energie, Hahn-Meitner Platz 1, 14109 Berlin, Germany
[2] J-PARC Center, Japan Atomic Energy Agency, Tokai, Ibaraki 319-1195, Japan
[3] Consiglio Nazionale delle Ricerche, Istituto dei Sistemi Complessi, Via Madonna del Piano 10, Sesto Fiorentino 50019, Italy
[4] INFN Sezione di Firenze, Via Madonna del Piano 10, Sesto Fiorentino 50019, Italy

[a)] Author to whom correspondence should be addressed: oriol.sans_planell@helmholtz-berlin.de

ABSTRACT

This study presents a significant development in the Energy-Resolved Neutron Imaging System RADEN, in the Japan Proton Accelerator Research Complex, Japan. Through a systematic study, the collimation power of the facility was reevaluated. What was initially considered to be values of 230, 420, and 760 have been proven to be much higher. To perform the calculation of the L/D factor of the beam, a state-of-the-art method has been used, along with a standard reference sample to measure the resolution of neutron images. To add robustness to the results, the study compares five different scintillators of different composition and thickness [^{6}LiF:ZnS(Ag) of 50, 100, 200, and 300 μm and Gd_2O_2S of 50 μm]. The calculated collimating power of the beam ranges between 470 and 1520. These results place a spotlight on an existing discrepancy between the geometrically calculated L/D and the actual measurable quantity, as well as highlight the superior performance of the RADEN beamline.

I. INTRODUCTION

Neutron imaging is an invaluable technique for materials science, engineering, and cultural heritage, among other fields,[1–4] due to its capabilities of inspecting through dense materials and providing insights on internal structures. The Energy-Resolved Neutron Imaging System RADEN, in the Japan Proton Accelerator Research Complex (J-PARC), is the current state-of-the-art pulsed neutron facility, bringing capabilities for advanced techniques related to neutron imaging and tomography.

One key parameter of any neutron imaging facility is the collimation power, represented by the L/D factor. This is one of the most relevant factors when quantifying the spatial resolution and image quality that the facility can provide. Before this study, RADEN had been characterized, by theoretical calculations and experimental measurements, with L/D values ranging from 230 up to 7500.[5–7] In an aim to improve the precision of collimation power measurements, a re-evaluation campaign was performed. This paper presents the results of a comprehensive experiment designed to measure, as accurately as possible, the L/D factor on RADEN's first three configurations, originally characterized with collimations of 230, 420, and 760, respectively.

The experimental approach to determine the collimation employed scintillator screens of varying thickness, as parameters such as the collimating power of the beam are independent of the detector system. The sample was a standard reference gadolinium knife edge, which was completely opaque to the neutron beam, making it a prime sample for the analysis of resolution by means of the Modulation Transfer Function (MTF). By placing the sample at different distances from the scintillator, it was possible to mathematically extract the value of the beam's collimation power.

The findings of this study reveal an unexpected and significant improvement in RADEN's collimation power compared to the previous estimation. This paper details the experimental methodology, presents the results, and provides an explanation of the discrepancy with the previous measurements.

II. METHODOLOGY

The beamline RADEN has a total of seven pin-hole configurations, which can be seen in Ref. 5. Due to constraints in space and time available for the experiment, only the first three configurations were studied (named Open-1, Open-2, and Open-3). These three configurations had an expected L/D of 230, 420, and 760, respectively, obtained by the usage of three different pin-hole systems of 100, 50.1, and 26.4 mm. The pin-holes for positions 2 and 3 are placed at 3.1 and 4.3 m from the source, respectively, while there is no specific pin-hole for configuration 1, just the opening of the neutron guide itself. To have robust results, five different scintillators were compared: four lithium fluoride [^{6}LiF:ZnS(Ag)] scintillators and one gadolinium oxide (Gd_2O_2S, also referred to as "Gadox"). The four LiF scintillators had thicknesses of 50, 100, 200, and 300 μm, while the Gadox was 50 μm in thickness. All scintillators are manufactured by RC TRITEC AG. The energy range for the neutron beam was limited to wavelengths >2 Å to maximize the absorption by the gadolinium sample. The effective pixel size of the camera was 47.5 μm.

The procedure followed to measure the L/D of the facility in each configuration has been the one proposed by Kaestner *et al.* in Ref. 8. The mathematics shown in the referenced article will be replicated in the Appendix. A reference sample is placed at different distances from the scintillator, and by measuring the image resolution on the sample at the different distances, it is possible to calculate the collimating power of the beam. The sample chosen for the measurements is a gadolinium knife edge of 100 μm thickness, which provides over 99% absorption in the thermal and cold energy range. It is the same sample used for Ref. 9, which is a prime sample to use the modulation transfer function (MTF) technique on to derive the image resolution.[10]

The distances at which the sample was placed for the resolution measurements with respect to the detector are shown in Table I. The table also presents the theoretical value that was expected to be measured, considering the geometry of the beam and the previous measurements done. The "Configuration" tab refers to the three operating configurations, Open 1–3, available at the facility. The resolution curve for each L/D configuration always follows the same trend, according to the equations present in the Appendix: the squared combination of a baseline value, the detector, plus a slope determined by the L/D itself. This creates an "elbow" on the curve, followed by a constant slope. The distances chosen for the experiment sought to get enough points in each of the two sections. To maintain a consistent intensity of the open beam and optimize the statistical quality of the images, the exposure times varied for each scintillator and configuration, following the values described in Table II.

TABLE I. The three configurations used in RADEN, along with the expected L/D value and the distances that were used between the detector and sample to measure the collimation power.

Configuration[a]	Expected L/D	Distances (mm)[b]
1	230	10, 20, 30, 50, 70, 90, 110, 140, 170, 210
2	420	10, 30, 60, 90, 130, 170, 210, 260, 310, 410
3	760	10, 110, 210, 310, 410, 510, 610

[a]Referred to, in previous literature, as "Open."
[b]Distance between the scintillator screen and the sample.

TABLE II. The exposure times used for each configuration and detector. The exposure times were tuned to optimize image statistics without saturating the detector. All measurements were performed with a beam power of 946 kW.

	Config. 1 (s)	Config. 2 (s)	Config. 3 (s)
LiF-50 μm	88	208	600
LiF-100 μm	60	140	400
LiF-200 μm	40	120	360
LiF-300 μm	24	72	240
Gadox-50 μm	360	840	...

III. RESULTS AND DISCUSSION

A. Different performance of scintillators

Different scintillators yield different results when measuring image resolution. When studying the beam's collimating power, the impact of the scintillator is shown as a variation on the baseline of the curve but there should be little to no impact regarding the value of L/D, which determines the subsequent slope of the curve. For this matter, performing the measurements with five different scintillators (four LiF-based and one GdOx) brought upon a means of validating the results of the collimating power of the beam. A side-by-side comparison between the three configurations used can be found in Fig. 1. Since the GdOx scintillator was only studied in configurations 1 and 2 and the results are compatible with the rest, it was excluded from the graphs of the figure but it is present in the supplementary material. From the plots in Fig. 2, it is apparent that the behavior of the scintillators is the expected: There is a variation at the baseline, which is due to the thickness of each scintillator but the slope of each curve is compatible within the error.

B. Calculation of L/D

To extract the L/D value from the measurements, the procedure detailed in Appendix has been employed. The results from the calculation are presented in Table III. The results present different observations to be noted:

1. The L/D values are very coherent across scintillators, and so are the values for the detector's contribution, all within the error in each configuration.
2. The values for collimation power differ greatly from those theoretically expected and measured in previous studies.

Addressing the first point, the coherence of the results is a testimony to both the stability and flexibility of the facility and the robustness of the method. Each individual scintillator presents a different value as baseline but the values for the beam collimation power are compatible in all configurations.

Combining the results present in Table III, the final values for the L/D in RADEN on the three configurations can be derived by calculating the average of all values and combining the error. The results presented in Table IV showcase the superior performance of RADEN as a neutron imaging beamline, placing its performance

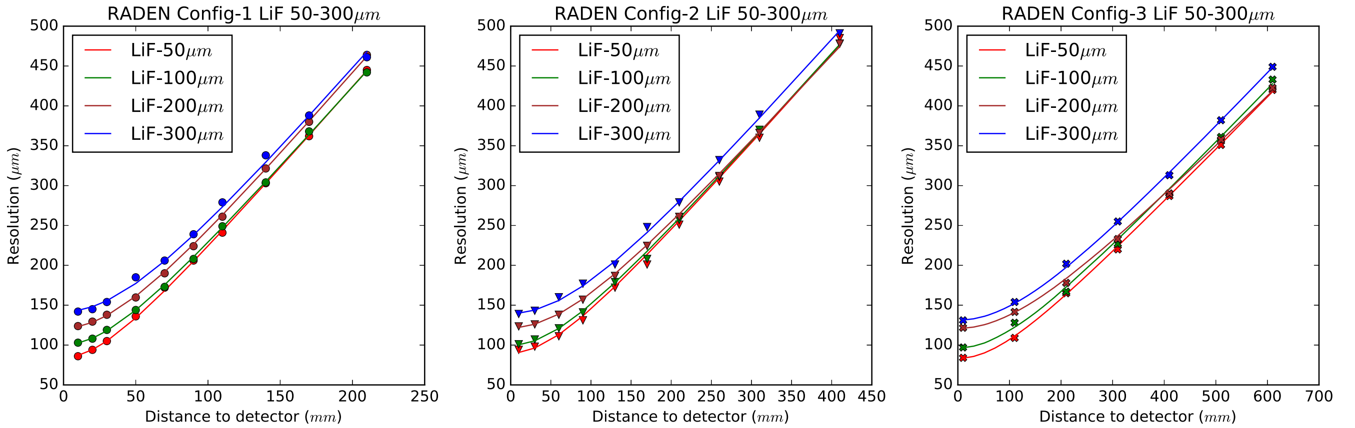

FIG. 1. The three plots represent the measurements taken in the three respective configurations, changing pin-holes in size and position to achieve three theoretical values of L/D of 230, 420, and 760. Due to the large amount of points present in the picture and the fit, the errors of the measure were removed from the figures but have been taken into account for each calculation and are present in the individual curves of the supplementary material, in which high-quality plots of each individual curve are present, along with their respective detector contribution and slopes.

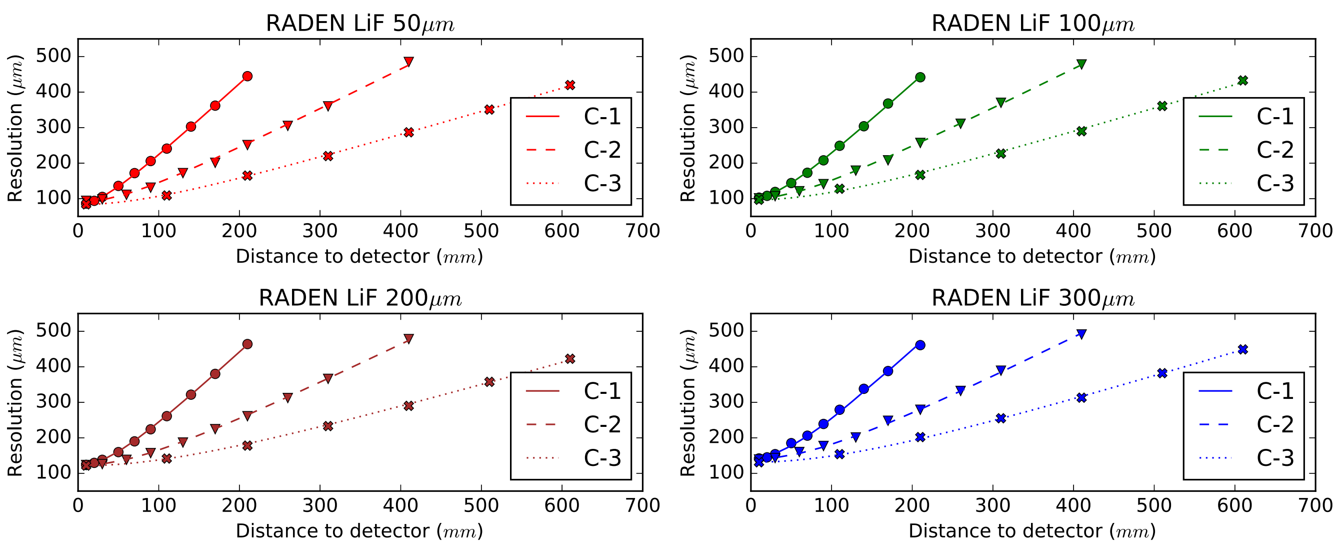

FIG. 2. The figure presents the same data shown in Fig. 1, but divided by scintillators, instead of configurations. This way, the change in performance between the different configurations (named C- in these plots for convenience) is more apparent. The facility has very stable behavior on each configuration, regardless of the scintillator used. The errors are not shown in this figure to increase the focus on the data points and the fit of each curve. The errors are present in each individual dataset present in the supplementary material.

high above what was reported until now, given the flux and resolution capabilities were considered for a much smaller collimation power.

The results obtained greatly differ from what was previously published in Refs. 5–7. This discrepancy can be traced to the sample used to perform the resolution measurements. As seen in Fig. 3, the sample originally used to measure the resolution and collimation power had a 50% transmission to the beam, which in turn created a bias when calculating the MTF. This situation is not encountered with the new reference sample, which is completely opaque to cold and thermal neutrons.

The geometrical calculation can hardly quantify the collimating power of a neutron beam. As shown in Ref. 12, many factors can influence the angular distribution of a neutron beam, and the lesser-present tails of a distribution can be hidden under the noise of the images taken with the detector. Our hypothesis, given the results shown in this article, is that the complex transport system composing RADEN and bringing the beam from the target to the

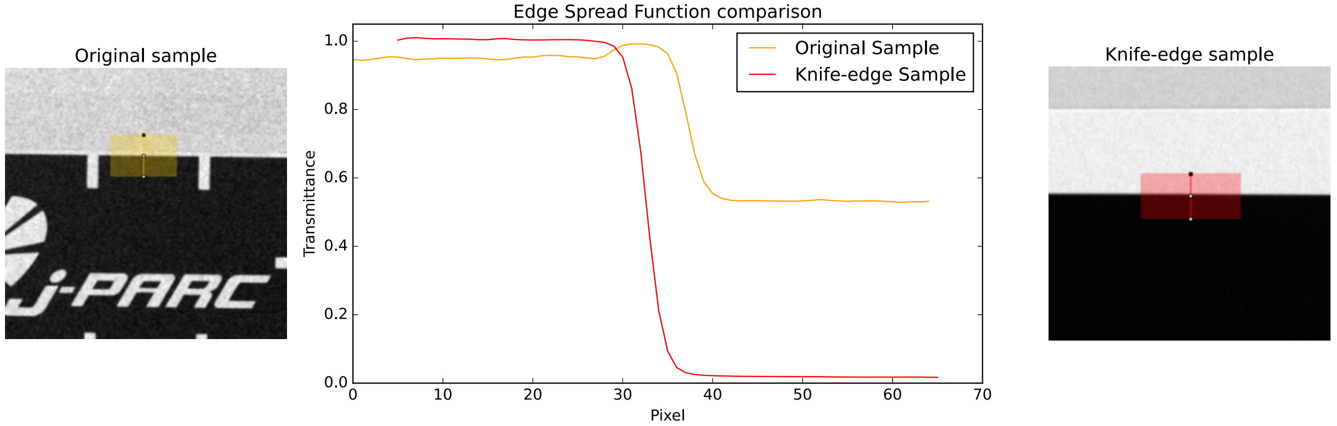

FIG. 3. On the left, the former sample, in which an area similar to that presented in a previous publication,[5] has been highlighted for reproducibility of results. The image to the right corresponds to the new knife-edge reference sample, with the red selection being the area chosen to plot the Edge Spread Function. The plot in the middle combines the two measurements, with corresponding colors for the two curves. Since the MTF is susceptible to the slope of the ESF, having only half the opacity directly impacts the evaluation of the resolution.

TABLE III. Values of beam collimation power and baseline calculated for each scintillator and each corresponding configuration. The errors presented have been derived by means of a Monte Carlo error propagation,[11] taking into account instrumental error (half a pixel) and MTF calculation error.

Scintillator	Configuration	Collimation power (L/D)	Baseline[a] (μm)
LiF-50 μm	1	481 ± 20	84 ± 24
	2	877 ± 38	90 ± 24
	3	1490 ± 72	83 ± 24
LiF-100 μm	1	486 ± 22	100 ± 24
	2	879 ± 38	100 ± 24
	3	1465 ± 74	96 ± 24
LiF-200 μm	1	470 ± 22	121 ± 24
	2	894 ± 42	122 ± 24
	3	1521 ± 86	121 ± 24
LiF-300 μm	1	471 ± 22	142 ± 24
	2	864 ± 40	140 ± 24
	3	1423 ± 74	131 ± 24
GdOx-50 μm	1	479 ± 22	80 ± 24
	2	872 ± 38	82 ± 24

[a]The error is mainly due to the pixel size of 47.5 μm.

TABLE IV. Values for the collimation power are calculated by averaging the four LiF scintillators and the GdOx when applicable. The error is calculated by combining the associated error of each measurement.

Configuration	Collimation power (L/D)	Error
1	477	±10
2	877	±18
3	1478	±38

instrument includes elements, such as neutron guides and secondary collimators, which alter the angular distribution of the beam to a degree that hides the actual L/D that can be measured experimentally within the image noise. The scope of this article is not to dig out the root cause of this discrepancy but to shed light, with data, on an issue that requires further study with high-fidelity simulations and more extended measurements on the remaining collimation configurations available in the facility.

SUPPLEMENTARY MATERIAL

The supplementary material contains all the plots related to each combination of scintillator and beam configuration used in the article, along with a graphic representation of the calculation for collimating power and detector baseline. The material is organized by beam configuration and a table is provided to organize all the graphs.

ACKNOWLEDGMENTS

The experiment has been performed within MLF proposal Grant No. 2023B0121.

AUTHOR DECLARATIONS

Conflict of Interest

The authors have no conflicts to disclose.

Author Contributions

Oriol Sans-Planell: Conceptualization (lead); Formal analysis (lead); Investigation (equal); Methodology (equal); Software (lead); Validation (equal); Writing – original draft (lead); Writing – review & editing (equal). **Takenao Shinohara**: Conceptualization (equal); Investigation (equal); Methodology (equal); Project administration (lead); Resources (lead); Validation (equal); Writing – review & editing (lead). **Francesco Grazzi**: Conceptualization (equal); Formal analysis (equal); Investigation (equal); Project administration (lead); Validation (lead); Writing – review & editing (lead). **Francesco Cantini**: Data curation (equal); Formal analysis (equal); Investigation (equal); Resources (supporting); Validation (equal). **Yuhua Su**: Investigation (equal); Resources (equal). **Yoshihiro Matsumoto**: Investigation (equal); Resources (equal). **Joseph D. Parker**: Investigation (equal); Resources (equal). **Ingo Manke**: Funding acquisition (equal); Resources (equal); Supervision (supporting); Writing – review & editing (equal).

DATA AVAILABILITY

The data that support the findings of this study are available from the corresponding author upon reasonable request.

APPENDIX: CALCULATION OF THE L/D

The measured resolution is the result of a combination of two effects: the detectors resolution limit σ_{det} and the penumbra blurring σ_{pen}. Those two values are combined as follows: $\sigma_{res} = \sqrt{\sigma_{pen}^2 + \sigma_{det}^2}$.

For this development, the following variable is defined: $C = D/L$. The penumbra blurring in this model is defined as $\sigma_{pen} = lC$. This definition is a good approximation when using a far pinhole. Considering this relation, the following equation stands:

$$\sigma_{res}(l)^2 = \sigma_{det}^2 + (lC)^2. \tag{A1}$$

Performing a series of measurements, the following system of linear equations is defined:

$$\begin{gathered} \sigma_{det}^2 + (l_1 C)^2 = \sigma_1^2 \\ \sigma_{det}^2 + (l_2 C)^2 = \sigma_2^2 \\ \vdots \\ \sigma_{det}^2 + (l_n C)^2 = \sigma_n^2, \end{gathered}$$

where $i = 1, \ldots, n$ identifies the measurement number. The notation of σ_{res} is simplified in each measurement as $\sigma_{1...n}$. The system of equations can be written in matrix form as

$$\begin{pmatrix} 1 & l_1 \\ 1 & l_2 \\ \vdots & \vdots \\ 1 & l_n \end{pmatrix} \begin{pmatrix} \sigma_{det}^2 \\ C^2 \end{pmatrix} = \begin{pmatrix} \sigma_1^2 \\ \sigma_2^2 \\ \vdots \\ \sigma_n^2 \end{pmatrix}. \tag{A2}$$

The least squared solution of this system is $\theta = (H^T H)^{-1} H^T x$. This estimate generates an approximately straight line, proportional to the L/D factor, with an asymptotic minimum toward the value of σ_{det}. To improve the precision of the calculation on the lower distances, a weighting function is applied to force the system to focus on those points, rather than the long-distance ones. The weight matrix takes the following form:

$$W = \begin{pmatrix} \frac{1}{l_1} & 0 & \cdots & 0 \\ 0 & \frac{1}{l_2} & \cdots & 0 \\ \vdots & \vdots & \ddots & \vdots \\ 0 & 0 & \cdots & \frac{1}{l_n} \end{pmatrix}. \tag{A3}$$

Modifying the result of the estimate to

$$\theta = (H^T W H)^{-1} H^T W x. \tag{A4}$$

From this equation, the results of θ are separated as $\theta_1 = \sigma_{det}^2$ and $\theta_2 = C^2$, which, considering the definition change at the beginning of this calculation, can be expressed as

$$\theta_2 = C^2 = (L/D)^{-2}. \tag{A5}$$

REFERENCES

[1] N. Kardjilov, I. Manke, R. Woracek, A. Hilger, and J. Banhart, "Advances in neutron imaging," Mater. Today **21**, 652–672 (2018).

[2] E. Lehmann, D. Mannes, A. Kaestner, and C. Grünzweig, "Recent applications of neutron imaging methods," Phys. Procedia **88**, 5 (2017).

[3] N. Kardjilov, I. Manke, A. Hilger, M. Strobl, and J. Banhart, "Neutron imaging in materials science," Mater. Today **14**, 248–256 (2011).

[4] N. Kardjilov, E. Lehmann, M. Strobl, R. Woracek, and I. Manke, "Neutron imaging," in *Neutron Methods for Archaeology and Cultural Heritage* (Springer, 2017), pp. 329–349.

[5] T. Shinohara, T. Kai, K. Oikawa, T. Nakatani, M. Segawa, K. Hiroi, Y. Su, M. Ooi, M. Harada, H. Iikura *et al.*, "The energy-resolved neutron imaging system, RADEN," Rev. Sci. Instrum. **91**, 043302 (2020).

[6] T. Shinohara, T. Kai, K. Oikawa, M. Segawa, M. Harada, T. Nakatani, M. Ooi, K. Aizawa, H. Sato, T. Kamiyama *et al.*, "Final design of the energy-resolved neutron imaging system 'RADEN' at J-PARC," J. Phys.: Conf. Ser. **746**, 012007 (2016).

[7] T. Shinohara and T. Kai, "Commissioning start of energy-resolved neutron imaging system, RADEN in J-PARC," Neutron News **26**, 11–14 (2015).

[8] A. Kaestner, Z. Kis, M. Radebe, D. Mannes, J. Hovind, C. Grünzweig, N. Kardjilov, and E. Lehmann, "Samples to determine the resolution of neutron radiography and tomography," Phys. Procedia **88**, 258–265 (2017).

[9] O. Sans-Planell, F. Cantini, M. Costa, E. Durisi, F. Grazzi, E. Mafucci, V. Monti, R. Bedogni, Y. Li, and L. van Eijck, "Improved methodologies to study the performance of the ANET Compact Neutron Collimator," Nucl. Instrum. Methods Phys. Res., Sect. A **1052**, 168260 (2023).

[10] G. D. Boreman, *Modulation Transfer Function in Optical and Electro-Optical Systems* (SPIE Press, Bellingham, WA, 2001), Vol. 4.

[11] J. F. Ogilvie, "A Monte-Carlo approach to error propagation," Comput. Chem. **8**, 205–207 (1984).

[12] O. Sans-Planell, F. Cantini, M. Costa, F. Grazzi, M. Morgano, and M. Yamada, "Study and perspective on neutron beam divergence improvement achievable by the combination of two or more neutron collimating systems," J. Phys.: Conf. Ser. **2605**, 012012 (2023).